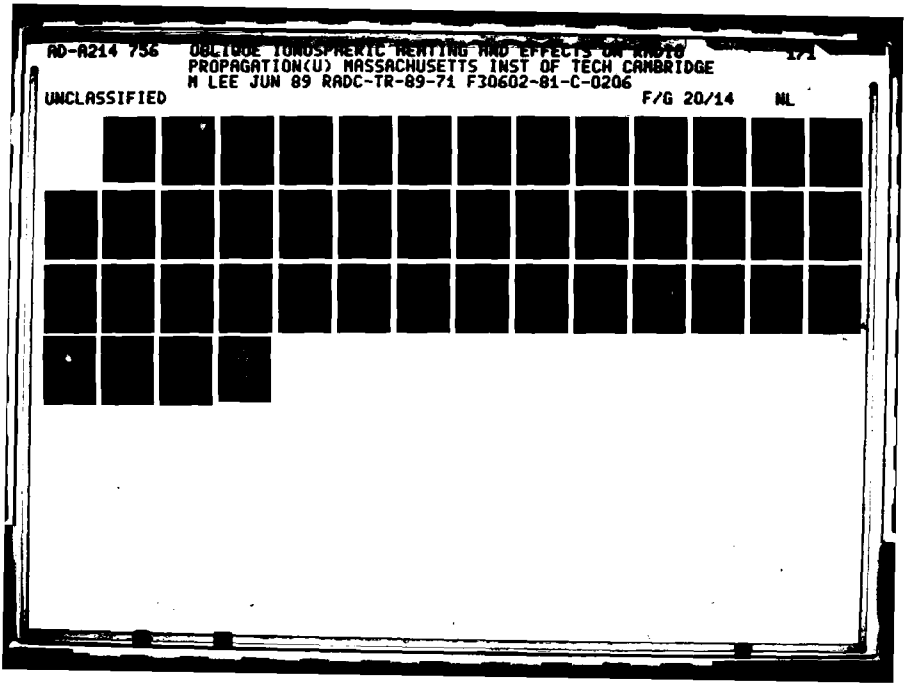
AD-A214 756
OBLIQUE IONOSPHERIC HEATING AND EFFECTS ON RADIO
PROPAGATION(U) MASSACHUSETTS INST OF TECH CAMBRIDGE
M LEE JUN 89 RADC-TR-89-71 F30602-81-C-0206
UNCLASSIFIED
F/G 20/14
NL

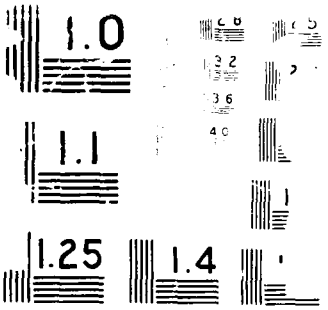
1.0
1.1
1.25
1.4

RADC-TR-89-71
Final Technical Report
June 1989

OBLIQUE IONOSPHERIC HEATING AND EFFECTS ON RADIO PROPAGATION

Massachusetts Institute of Technology

Min-Chang Lee

ROME AIR DEVELOPMENT CENTER
Air Force Systems Command
Griffiss Air Force Base, NY 13441-5700

This report has been reviewed by the RADC Public Affairs Division (PA) and is releasable to the National Technical Information Service (NTIS). At NTIS it will be releasable to the general public, including foreign nations.

RADC-TR-89-71 has been reviewed and is approved for publication.

APPROVED: Stanford P. Yukon

STANFORD P. YUKON
Project Engineer

APPROVED: John K. Schindler

JOHN K. SCHINDLER
Director of Electromagnetics

FOR THE COMMANDER: John A. Ritz

JOHN A. RITZ
Directorate of Plans & Programs

If your address has changed or if you wish to be removed from the RADC mailing list, or if the addressee is no longer employed by your organization, please notify RADC (EECP) Hanscom AFB MA 01731-5000. This will assist us in maintaining a current mailing list.

Do not return copies of this report unless contractual obligations or notices on a specific document require that it be returned.

UNCLASSIFIED

SECURITY CLASSIFICATION OF THIS PAGE

REPORT DOCUMENTATION PAGE

Form Approved OMB No. 0704-0188

1a. REPORT SECURITY CLASSIFICATION: UNCLASSIFIED	1b. RESTRICTIVE MARKINGS: N/A
2a. SECURITY CLASSIFICATION AUTHORITY: N/A	3. DISTRIBUTION/AVAILABILITY OF REPORT: Approved for public release; distribution unlimited.
2b. DECLASSIFICATION/DOWNGRADING SCHEDULE: N/A	
4. PERFORMING ORGANIZATION REPORT NUMBER(S): N/A	5. MONITORING ORGANIZATION REPORT NUMBER(S): RADC-TR-89-71
6a. NAME OF PERFORMING ORGANIZATION: Massachusetts Institute of Technology; 6b. OFFICE SYMBOL (If applicable):	7a. NAME OF MONITORING ORGANIZATION: Rome Air Development Center (EECP)
6c. ADDRESS (City, State, and ZIP Code): Cambridge MA 02139	7b. ADDRESS (City, State, and ZIP Code): Hanscom AFB MA 01731-5000
8a. NAME OF FUNDING/SPONSORING ORGANIZATION: Rome Air Development Center; 8b. OFFICE SYMBOL (If applicable): EECP	9. PROCUREMENT INSTRUMENT IDENTIFICATION NUMBER: F30602-81-C-0206
8c. ADDRESS (City, State, and ZIP Code): Hanscom AFB MA 01731-5000	10. SOURCE OF FUNDING NUMBERS: PROGRAM ELEMENT NO: 62702F; PROJECT NO: 4600; TASK NO: 16; WORK UNIT ACCESSION NO: P6

11. TITLE (Include Security Classification)

OBLIQUE IONOSPHERIC HEATING AND EFFECTS ON RADIO PROPAGATION

12. PERSONAL AUTHOR(S)
Min-Chang Lee

13a. TYPE OF REPORT	13b. TIME COVERED	14. DATE OF REPORT (Year, Month, Day)	15. PAGE COUNT
Final	FROM May 87 TO Sep 87	June 1989	46

16. SUPPLEMENTARY NOTATION

17. COSATI CODES			18. SUBJECT TERMS (Continue on reverse if necessary and identify by block number)
FIELD	GROUP	SUB-GROUP	
20	14		Oblique Ionospheric Modification

19. ABSTRACT (Continue on reverse if necessary and identify by block number)

The process of self focusing of high intensity Gaussian HF electromagnetic beams in the ionosphere is studied. Analytic expressions for threshold intensity, growth rate and focal length are obtained in terms of the beam parameters for self focusing due to the ponderomotive force.

Spectral broadening of VLF waves traversing the ionosphere has been studied. Two mechanisms, nonlinear scattering and parametric excitation of lower hybrid waves are shown to provide nonlinear mode conversion of VLF waves into electrostatic plasma modes in the presence of ionospheric density striations. The proposed mechanisms can be tested in an experiment that combines the operation of HF and VLF ionospheric heaters.

20. DISTRIBUTION/AVAILABILITY OF ABSTRACT	21. ABSTRACT SECURITY CLASSIFICATION
☒ UNCLASSIFIED/UNLIMITED ☐ SAME AS RPT ☐ DTIC USERS	UNCLASSIFIED
22a. NAME OF RESPONSIBLE INDIVIDUAL: Stanley J. Muhar	22b. TELEPHONE (Include Area Code): (617) 377-2985; 22c. OFFICE SYMBOL: RADC/EECP

DD Form 1473, JUN 86 — Previous editions are obsolete

SECURITY CLASSIFICATION OF THIS PAGE
UNCLASSIFIED

Final Report to Rome Air Development Center for Sponsored Research in "Oblique Ionospheric Heating and Effects on Radio Propagation" during May 14 - September 30, 1987. Prepared by

Dr. Min-Chang Lee
Principal Investigator

1. Introduction

Preliminary research under the sponsorship of the RADC has been actively conducted at Massachusetts Institute of Technology in the following three areas: (1) Self-focusing of high power radio waves traversing the ionosphere, (2) Nonlinear scattering of radio waves off the ionospheric density striations, and (3) Enhanced ionospheric heating by the combined operation of two heaters. Briefly described as follows is the research progress in these projects.

2. Self-focusing of radio waves

A graduate student, H.C. Han, has analyzed the self-focusing of a Gaussian radio wave beam propagating through a uniform, magnetized plasma under the supervision of Dr. Min-Chang Lee. This work, when applied to the ionospheric radio propagation, offers the following scenario. The radio waves injected from a ground-based transmitter can be approximated as plane waves during their transionospheric propagation. Through the filamentation instability (Lee and Kuo, Radio Science, 1985), wave-like ionospheric density fluctuations can be excited and, consequently, break the radio wave beam into filaments. These filaments can be approximately described by Gaussian radio wave beams.

The self-focusing process under consideration arises from the radio wave-ionospheric plasma interactions that yield nonlinear forces acting primarily on electrons. These forces may cause the increasing of ionospheric plasma dielectric constant along the radio wave path and results in the focusing of radio waves. The nonlinear forces induced by radio waves are the thermal pressure force and the ponderomotive force. These nonlinear forces work additively in causing the self-focusing of radio waves though one may become dominant

over the other under certain ionospheric conditions. For instance, the thermal pressure force is the dominant force when the scale lengths of induced plasma density fluctuations along the geomagnetic field line exceeds several electron mean free paths.

Under the self-focusing process, the shape of a radio wave beam can be altered. More specifically, a Gaussian radio wave beam will change its field intensity profile during the transionospheric propagation. The enhanced field intensity near the beam center due to the self-focusing process can result in intense electron heating and lead to the generation of hot spots in the ionosphere. As the first step in our theoretical analysis of the problem, we only consider the ponderomotive force effect for simplicity. The threshold power of the concerned process is determined by the balance between the natural diffraction and the self focusing process. It depends upon the initial beam width, the nonlinear dielectric constant, and the wave number.

Solving the nonlinear wave equation, we can clearly see the trend of the spatial evolution of the wave field intensity profile, namely, a Gaussian radio wave beam does not maintain its shape during the self-focusing process in the ionosphere. If we ignore the saturation processes, the focal length can be defined to be the propagation distance before the wave field intensity reaches infinity due to the self-focusing effect. This theoretical focal length represents the upper bound of the characteristic path length for the self-focusing process to accomplish. Since the thermal pressure force and the ponderomotive force contribute additively to the self-focusing of radio waves, our calculated threshold power is apparently overestimated because in our formulation of the theory we ignore the effect of the thermal pressure force. However, interestingly enough, our threshold power has the same order of magnitude as that found by the numerical work of Bernhardt and Duncan (JATP, 1982) who, by contrast, neglect the effect of the ponderomotive force. In our future analytical study of the self-focusing process, we shall include the thermal pressure force to obtain a complete physical picture of the concerned process. Attached with the report as the Appendix A is the preprint of a proceedings paper that will be published by the Ionospheric Effects Symposium held during 5 - 7 May, 1987.

3. Nonlinear scattering of radio waves in the ionosphere

A nonlinear scattering process has been analyzed by Keith M. Groves, another graduate student of Dr. Min-Chang Lee to show the nonlinear mode conversion of radio waves into electrostatic plasma modes in the presence of ionospheric density striations. This work was motivated by the observations of the spectral broadening of monochromatic VLF radio signals traversing the ionosphere conducted in the so-called VLF wave injection experiments (Bell et al., 1983).

According to Bell et al. (1983), a bandwidth expansion as large as 100 Hz was experienced by a nearly monochromatic signal at 13.6 KHz ± 1 Hz injected from a ground-based VLF transmitter as the signal traversed the ionosphere and reached the satellite altitudes in the range of 600–3800 kilometers. In other words, the expansion of bandwidth as large as 1% of the carrier frequency was observed in the transionospheric propagation of VLF waves. The off-carrier components are believed to be electrostatic in nature (Inan and Bell, 1985). This phenomenon occurs only in the presence of impulsive VLF hiss and/or a lower hybrid resonance (LHR) noise band with an irregular cutoff frequency, and only for signals whose frequencies exceed the LHR frequency at the satellite location.

Two mechanisms have been proposed to explain the spectral broadening phenomenon. One is the nonlinear scattering process of VLF signals by the existing ionospheric density fluctuations that renders the nonlinear mode conversion of VLF waves into lower hybrid waves. The scattering of VLF waves by ionospheric density fluctuations causes elliptically polarized modes. However, we find that the induced elliptically polarized modes may become predominantly electrostatic. They occur when the scale lengths of ionospheric density irregularities are much less than the VLF wavelength. We note that the scattered VLF waves, therefore, have a broadened wave vector spectrum that can give rise to the Doppler shift of the VLF waves as the moving satellite sensed.

The other proposed mechanism suggests parametric instabilities that can produce a spectrally broadened signal. The injected VLF wave excites both the Stokes and anti-Stokes components of lower hybrid waves, concomitantly, producing a field-aligned purely growing mode Lee and Kuo, 1984). The Doppler shift of the sidebands relative to the whistler pump wave created a spectrally broadened signal. A paper submitted by the graduate student, Keith M. Groves and accepted already for the Student Prize Paper Competition in the 1988 National Radio Science Meeting, Boulder, Colorado is attached as the Appendix B of this report.

4. Enhanced ionospheric heating by two heaters

The other project conducted by Dr. Min-Chang Lee at MIT with the participation of graduate students, C.P. Liao, D.R. Rivas, and K.M. Groves is the theoretical analysis of enhanced ionospheric heating by the combined operation of two heaters. The proposed scenario is as follows. Illuminate the ionospheric F region by a vertically injected HF or MF heater wave first. Then, launch a VLF wave propagating through the HF or MF modified ionospheric region.

It has been known both theoretically and experimentally that short-scale (typically meter-scale) ionospheric density striations can be excited by a vertically injected HF or

MF wave from a ground-based transmitter in less than a second (Lee et al., 1986), while large-scale (say, hundreds of meter-scale) striations need tens of seconds to be excited. It is desirable to operate the HF or MF heater in a puised mode with a duration of, say, a few seconds to assure the favorable excitation of meter-scale rather than large-scale ionospheric density striations. As discussed in the previous section, the HF or MF wave induced meter-scale ionospheric density striations are able to nonlinearly scatter the subsequently launched VLF wave into a quasi-electrostatic mode, viz., a lower hybrid wave mode.

Several prominent ionospheric effects can be expected and tested experimentally. The most notable effects are associated with the generation of lower hybrid wave modes that can effectively accelerate electrons along the geomagnetic field. The electron acceleration leads to airglow (6300 A, 5577 A, ···) enhancement and, then, a broad height distribution of plasma lines that can be measured by incoherent backscatter radars. Presented in Appendix C is the research progress in this work.

The further theoretical investigation of this project shall be pursued and extended to the case that the HF waves are injected obliquely from a ground-based transmitter. Collaboration with Dr. Stanford Yukon of RADC is expected. Dr. Yukon's ionospheric radio research group has been actively planning an oblique ionospheric heating experiment with other Air Force research groups and universities. During the oblique ionospheric heating by an HF wave, the short-scale ionospheric density striations cannot be excited because the radio wave-ionospheric plasma resonance conditions cannot be matched for the excitation of parametric decay instability. However, relatively large scale (> tens of meters) ionospheric density striations can be generated via other plasma instabilities such as filamentation instability/self-focusing instability, Brillouin instability, and Raman instability. Hence, in principle, these instabilities are still capable of converting the VLF waves into lower hybrid waves via the nonlinear scattering process.

The calculation of wave field intensities in the caustic region of an obliquely propagating HF wave were carried out by Field and Warber (1985). Their calculations show that a transmitter having a power-gain product of 5 MW can launch an oblique wave strong enough to produce electric fields of several tenths of a volt per meter or more in the caustic region. If the wave field intensities are indeed so intense as Field and Warber (1985) indicate, strong ohmic heating of electrons can be expected. Nevertheless, in the recent oblique experiment conducted in Maine by AFGL, RADC, University of Lowell, and MIT, no indication of electron heating was seen. We shall look into this problem in the near future for the oblique heating experiments currently being planned by the RADC and AFGL.

5. Presentation of research results in conferences

Two trips made for attending conferences were supported by the RADC contract. One was the trip to Springfield, Virginia in May, 1987 made by Dr. Min-Chang Lee with four students to present five papers in the Ionospheric Effects Symposium. The other trip was made by Dr. Min-Chang Lee alone to Vancouver, Canada for delivering an invited talk at the IAGA General Assembly in August, 1987.

References

Bell, T.F., H.G. James, U.S. Inan, and J.P. Katsufrakis, The apparent spectral broadening of VLF transmitter signals during transionospheric propagation, J. Geophys. Res., 88, 4813-4840, 1983.

Field, E.C. and C.R. Warber, Ionospheric heating with obliquely incident waves, Geophys. Res. Lett., 12, 761-763, 1985.

Lee, M.C. and S.P. Kuo, Production of lower hybrid waves and field-aligned plasma density striations by whistlers, J. Geophys. Res., 89, 10873, 1984.

Lee, M.C. and S.P. Kuo, Simultaneous excitation of large- scale geomagnetic field fluctuations and plasma density irregularities by powerful radio waves, Radio Sci., 20, 539, 1985.

APPENDIX A

THE SELF-FOCUSING OF A GAUSSIAN RADIO WAVE BEAM

Abstract

As a high-power radio wave beam propagates in the ionosphere, the nonlinear interactions between the wave and plasmas can lead to the self-focusing of the radio beam. The required threshold or critical power is determined by the balance between the natural diffraction and the self-focusing process. Solving the nonlinear wave equation near the wave beam center, we can obtain the focal length for the concerned process to accomplish. It has been shown that a Gaussian radio wave beam shall not maintain its shape during the self-focusing process in the ionosphere.

1. Introduction

The self-focusing of radio waves in space has received much attention in the research on ionospheric modification by high power radio waves. This phenomenon, has also been actively studied in optical media see, e.g. Chiao et al., 1964; Kelley, 1965; Lugovoĭ and Prokhorov, 1974 and references therein . In ionospheric plasmas, the self-focusing of radio waves arises from the wave-ionosphere interaction that yields nonlinear forces acting primarily on electrons. These forces may cause the increasing of ionospheric plasma dielectric constant along the radio wave path and results in the focusing of radio waves. The nonlinear forces induced by radio waves are the ponderomotive force and the thermal pressure force. When the scale length of plasma density perturbation along the geomagnetic field line exceeds several electron mean free

parts, the thermal pressure force dominates over the ponderomotive force in causing the self focusing instability.

Under the self-focusing process, the shape of a radio wave beam can be altered. More specifically, a Gaussian radio beam will change its field intensity profile through the transionospheric propagation. The purpose of the present work is to investigate analytically this problem. As the first step, we restrict ourselves on the ponderomotive force effect only. One can see the trend of the spatial evolution of the field intensity profile. The threshold field for the self-focusing process turns out to be dependent of the initial beam width, the nonlinear dielectric constant, and the wave number. From the analysis of the intensity profile, certain assumptions made in solving the wave equation, such as the expansion of the field intensity as a function of ρ^2 near the beam center, and the neglect of the diffraction effect, can be justified.

2. Nonlinear Wave-Ionosphere Interactions

When a high power radio wave beam propagates in the ionosphere, the radiation pressure gives rise to a nonlinear force, known as the *ponderomotive force*, acting basically on electrons, if the wave frequency is much higher than the ion plasma frequency. The ponderomotive force acting on an electron is given by

$$f_{NL} = -\frac{e^2}{4m_e\omega^2}\nabla A^2 \qquad (1)$$

where A is the amplitude of the wave electric field, $E = A(r)\cos\omega t$. Since this force points in the direction opposite to that of ∇A^2, it is able to push the electrons out of the wave path.

An electron under the action of ponderomotive force feels an apparent electrical potential determined by

$$\phi_{ap} = \frac{e}{4m_e\omega^2}A^2 \qquad (2)$$

Under the conditions that A^2 is slowly varying in time, and it has a scale length much greater than the Debye

length, and that the plasma is locally thermalized, the Boltzmann relation in the presence of ponderomotive force can be written as

$$n = n_0 \exp\left[\frac{\epsilon^2 A^2}{4k_B(T_i + T_e)m_i\omega^2}\right] \quad (3)$$

where n_0 is the background electron density, k_B is the Boltzmann constant, T_i is ion temperature, and T_e is electron temperature. Therefore, the dielectric constant of the plasma is given by

$$\epsilon = \epsilon_0\left\{1 - \frac{\omega_{p0}^2}{\omega^2}\exp\left[\frac{\epsilon^2 A^2}{4k_B(T_i + T_e)m_i\omega^2}\right]\right\} \quad (4)$$

where ϵ_0 is the dielectric constant for free space, and ω_{p0} is the background electron plasma frequency. Assuming the wave frequency ω is much greater than the local electron plasma frequency ω_{p0}, we can express Eq. (4) as

$$\epsilon = \epsilon_p + \epsilon_2 + \epsilon_4 + \cdots \quad (5)$$

where

$$\epsilon_p = \epsilon_0\left(1 - \frac{\omega_{p0}^2}{\omega^2}\right) \quad (6)$$

$$\epsilon_2 = \frac{\epsilon_0\omega_{p0}^2\epsilon^2 A^2}{4k_B(T_i + T_e)m_i\omega^4} \quad (7)$$

The ϵ_p is identified to be the background dielectric constant and the higher order terms ϵ_2, ϵ_4...etc. are dependent upon the field intensity. For instance, the field intensity dependence in ϵ_2 can be shown to be

$$\epsilon_2 = \alpha_2 A^2 \quad (8)$$

where

$$\alpha_2 = \frac{\epsilon_0\omega_{p0}^2\epsilon^2}{4k_B(T_i + T_e)m_i\omega^4} \quad (9)$$

3. Nonlinear Wave Equation

Consider a powerful radio wave propagating in z direction. The wave equation is governed by

$$\nabla\left(E \cdot \frac{\nabla\epsilon}{\epsilon}\right) - \nabla^2 E - \mu_0\epsilon\frac{\partial^2}{\partial t^2}(\epsilon E) = 0 \quad (10)$$

If we assume that $\epsilon_p \gg \epsilon_2 \gg \epsilon_4 \gg \cdots$, we only need to retain the first two terms in Eq. (5). Then neglecting the first term in Eq. (10) yields

$$\nabla^2 \bar{E} + \mu_o \frac{\partial^2}{\partial t^2} (\epsilon \bar{E}) = 0 \qquad (11)$$

Let $\bar{E} = \mathcal{E}(r, t) \exp i(kz - \omega t)$, where $\mathcal{E}$ is the slowly-varying field amplitude vector, $k = \omega \sqrt{\mu_o \epsilon_p}$ is the unperturbed wave number and ω is the wave frequency. Then, we have

$$\nabla_\perp^2 \mathcal{E} + 2ik \frac{\partial \mathcal{E}}{\partial z} - \omega^2 \mu_o \epsilon_2 \mathcal{E} + \epsilon_p \mu_o \left(2i\omega \frac{\partial \mathcal{E}}{\partial t} + \frac{\partial^2 \bar{\mathcal{E}}}{\partial t^2} \right) + 2\mu_o \frac{\partial \epsilon}{\partial t} \left(i\omega \mathcal{E} + \frac{\partial \mathcal{E}}{\partial t} \right) + \mu_o \frac{\partial^2 \epsilon}{\partial t^2} \mathcal{E} = 0 \qquad (12)$$

The quantities Λ_z, $\Lambda_\perp$, λ, T and τ are defined, respectively, as the scale length of $\mathcal{E}$ along the z-axis, that perpendicular to z-axis, the wave length, the wave period, and the time scale of the temperal variation of $\mathcal{E}$. For simplicity, we consider a cylindrical wave beam with $T \sim \tau$ which implies the quasi stationary condition, and $\lambda \sim \Lambda_\perp \sim \Lambda$. The order of magnitude estimates of each term in Eq. (12) are made as follows:

$$\nabla_\perp^2 \mathcal{E} \sim \frac{1}{\Lambda^2} \mathcal{E};$$

$$\nabla^2 \mathcal{E} \sim \frac{1}{\Lambda^2} \mathcal{E};$$

$$2ik \frac{\partial \mathcal{E}}{\partial z} \sim i \frac{4\pi}{\lambda} \frac{1}{\Lambda^2} \mathcal{E};$$

$$\omega^2 \mu_o \epsilon_2 \mathcal{E} \sim \frac{4\pi^2}{\lambda^2} \frac{\epsilon_2}{\epsilon_p} \mathcal{E};$$

$$2i\epsilon\mu_o\omega \frac{\partial \mathcal{E}}{\partial t} \sim \frac{4\pi}{\lambda^2} \frac{T}{\tau} \mathcal{E};$$

$$\epsilon\mu_o \frac{\partial^2 \mathcal{E}}{\partial t^2} \sim \frac{1}{\lambda^2} \frac{T^2}{\tau^2} \mathcal{E};$$

$$2\mu_o \frac{\partial \epsilon}{\partial t} \frac{\partial \mathcal{E}}{\partial t} \sim \frac{4\pi}{\lambda^2} \frac{T}{\tau} \frac{\epsilon_2}{\epsilon_p} \mathcal{E};$$

$$2\mu_o \frac{\partial \epsilon}{\partial t} \frac{\partial \mathcal{E}}{\partial t} \sim \frac{2}{\lambda^2} \frac{T^2}{\tau^2} \frac{\epsilon_2}{\epsilon_p} \mathcal{E};$$

$$\mu_o \frac{\partial^2 \epsilon}{\partial t^2} \mathcal{E} \sim \frac{1}{\lambda^2} \frac{T^2}{\tau^2} \frac{\epsilon_2}{\epsilon_p} \mathcal{E}$$

Neglecting the higher order terms but keeping the transversal part of the first, the second and the third terms in Eq. (12) leads to

$$2ik \frac{\partial \mathcal{E}}{\partial z} + \nabla_\perp^2 \mathcal{E} - \frac{k^2 \epsilon_2}{\epsilon_p} \mathcal{E} = 0 \qquad (13)$$

4. Profile Evolution of Wave Field Intensity

Let $\mathcal{E} = A(\varrho, z)\exp i\varphi(\varrho, z)$. Substituting $\mathcal{E}$ into Eq. (13) and separating the real and imaginary parts of (13), we have the following two equations

$$2k\frac{\partial A}{\partial z} + 2\frac{\partial A}{\partial \varrho}\frac{\partial \varphi}{\partial \varrho} + A\frac{\partial^2 \varphi}{\partial \varrho^2} + \frac{A}{\varrho}\frac{\partial \varphi}{\partial \varrho} = 0 \qquad (14)$$

$$\frac{\partial^2 A}{\partial \varrho^2} + \frac{1}{\varrho}\frac{\partial A}{\partial \varrho} - 2kA\frac{\partial \varphi}{\partial z} - A\left(\frac{\partial \varphi}{\partial \varrho}\right)^2 + \frac{k^2\epsilon_2}{\epsilon_p}A = 0 \qquad (15)$$

expressed in the cylindrical coordinate system with azimuthal symmetry for a uniform, isotropic collisional plasma. These two equations can be rewritten as

$$k\frac{\partial A^2}{\partial z} = -\nabla_\perp \cdot (A^2\nabla_\perp \varphi) \qquad (16)$$

$$2k\frac{\partial \varphi}{\partial z} + (\nabla_\perp \varphi)^2 - \frac{\nabla_\perp^2 A}{A} + \frac{k^2\epsilon_2}{\epsilon_p} = 0 \qquad (17)$$

Eq. (17) can be further rewritten in the form of the Hamilton-Jacobi equation for the particle motion: $2\frac{\partial S}{\partial t} + (\nabla S)^2 - 2V = 0$, where $\frac{1}{2}(\nabla S)^2 - 2V$ is the Hamiltonian, ∇S is the momentum and V is the potential field (Wagner et al. 1968). We can specify the time with kz, the spatial coordinates with $k\varrho$, S with φ, and V with $-\frac{1}{2}\cdot\frac{\nabla_\perp^2 A}{k^2 A} + \frac{\epsilon_2}{\epsilon_p}$. The first term with V represents the diffraction effect and the second term represents the nonlinear effect (i.e. the focusing effect). From the Hamilton-Jacobi equation, we have

$$\frac{\partial^2 \varrho}{\partial z^2} = -\frac{\partial}{\partial \varrho}V \qquad (18)$$

where

$$V = -\frac{1}{2}\cdot\frac{\nabla_\perp^2 A}{k^2 A} + \frac{\epsilon_2}{\epsilon_p} \qquad (19)$$

This equation describes the radial position ϱ of a ray as a function of z on its trajectory, as an analogue to the particle motion in a potential field. The trend for the spatial evolution of the wave field intensity profile can then be seen.

Suppose that we have a Gaussian beam with the field intensity $A(\varrho) = A_m \exp\left(-\frac{\varrho^2}{2a^2}\right)$, where A_m is

the peak intensity, and w_o is the beam width. Since $\epsilon_2 = \mathcal{B}_2 A_m^2 \exp(-\frac{\varrho^2}{w_o^2})$ from Eq. (8), the potential V is, hence, a function of ϱ given by

$$V(\varrho) = \frac{1}{2k^2}\left[\frac{2}{w_o^2} - \frac{\varrho^2}{w_o^4} + \frac{\mathcal{B}_2}{\epsilon_p} A_m^2 e^{-\frac{\varrho^2}{w_o^2}}\right] \tag{20}$$

The first two terms on the right hand side represent diffraction while the third term represents the focusing effect. If V has a maximum at $\varrho = \varrho_{max}$, then the focusing effect is dominant for $\varrho < \varrho_{max}$, whereas the diffraction effect is dominant for $\varrho > \varrho_{max}$. The ϱ_{max} can be determined by taking the derivative of V with respect to ϱ as follows

$$\varrho_{max} = w_o \ln\left[\frac{k^2 w_o^2 \mathcal{B}_2 A_m^2}{\epsilon_p}\right] \tag{21}$$

The "critical power" for self-focusing can be defined by setting $\varrho_{max} = 0$ in Eq. (21), viz.,

$$(A_m^{cr})^2 = \frac{\epsilon_p}{k^2 w_o^2 \mathcal{B}_2} \tag{22}$$

Consider a Gaussian beam with $A_m \gg A_m^{cr}$ and a plane wave front (i.e. $\frac{\partial \varrho}{\partial z}_{z=0} = 0$). The portion of the beam at $\varrho < \varrho_{max}$ will be focused, while that at $\varrho > \varrho_{max}$ will be diffracted. In other words, an immediate redistribution of field intensity is expected. The shape of the beam will change from a Gaussian to one with a sharper center and higher wings.

In fact, for any field profile peaking at the center and dying out as ϱ gets large, we can do the local analysis near $\varrho = 0^+$. We can expand the field intensity profile in a series of ϱ for $\varrho = 0^+$. Then, this series can be written as $1 - \eta^n + \cdots$ after normalizing the first term and defining a new variable η. Substituting this series into Eq. (19), we can see that n can not be less than 2 to avoid the physically meaningless singularity of V at $\varrho = 0$. With this restriction, together with a high enough beam power, the focusing effect will dominate over diffraction near the beam center. Under the aforesaid conditions, it is then possible to solve Eq. (13) analytically near the beam center.

5. Self-Focusing Near The Beam Center

For simple mathematical manipulation, we express $\mathcal{E} = xe^{S(\varrho,z)}$ in Eq. (13), leading to the following two coupled equations

$$\frac{\partial^2 S_r}{\partial \varrho^2} + \frac{1}{\varrho}\frac{\partial S_r}{\partial \varrho} + \left(\frac{\partial S_r}{\partial \varrho}\right)^2 - \left(\frac{\partial S_i}{\partial \varrho}\right)^2 - 2k\frac{\partial S_i}{\partial z} - \frac{k^2 \beta_2}{\epsilon_p} e^{2S_r} = 0 \quad (23)$$

$$\frac{\partial^2 S_i}{\partial \varrho^2} + \frac{1}{\varrho}\frac{\partial S_i}{\partial \varrho} - 2\left(\frac{\partial S_r}{\partial \varrho}\right)\left(\frac{\partial S_i}{\partial \varrho}\right) - 2k\frac{\partial S_r}{\partial z} = 0 \quad (24)$$

where $S(\varrho, z) = S_r(\varrho, z) + iS_i(\varrho, z)$. If the wave power is much greater than the critical power, we can make the following approximations:

(i) The diffraction terms in Eq. (23) can be neglected as $\varrho \to 0^+$.

(ii) $S_r(\varrho, z) = a_0(z) + \varrho^2 a_2(z) + \varrho^4 a_4(z) + \cdots$

(iii) By assuming a spherical wave front, we have $S_i(\varrho, z) = b_0(z) + \varrho^2 b_2(z)$

Using the above expansions for S_r and S_i in Eqs. (23), (24) and collecting terms of the same order in ϱ, we then get a set of equations for a's and b's. If we neglect terms higher than the second order of ϱ, Eqs. (23), and (24) become

$$b_0' = \frac{k\beta_2}{2\epsilon_p} a_m \quad (25)$$

$$2b_2^2 + kb_2' = \frac{k^2 \beta_2}{\epsilon_p} a_m a_2 \quad (26)$$

$$a_m' + \frac{4}{k} b_2 a_m = 0 \quad (27)$$

$$a_2' + \frac{4}{k} b_2 a_2 = 0 \quad (28)$$

where $a_m \equiv e^{2a_0}$. If we define a function $g(z) \equiv \int^z b_2(z')dz'$, then Eqs. (26)-(28) have the forms of

$$2(g')^2 + kg'' = \frac{k^2 \beta_2}{\epsilon_p} c_m c_2 e^{-\frac{4}{k}g} \quad (26')$$

$$a_m = c_m e^{-\frac{4}{k}g} \quad (27')$$

$$a_2 = c_2 e^{-\frac{4}{k}g} \quad (28')$$

where c_m and c_2 are integration constants. The initial conditions are set to be

$$a_m(z=0) = A_{mo}^2 \tag{29}$$

$$a_2(z=0) = \frac{1}{2w_o^2} \tag{30}$$

$$a_1(z=0) = \frac{k}{2R} \tag{31}$$

where R is the initial curvature of wave front at $z = 0$, and $R > 0$ for a diverging beam, while $R < 0$ for a converging beam. Here, w_o is the initial beam width and A_{mo} is the initial peak field intensity. Then, Eq. (26') can be straightforwardly solved. In the following, we express our final results in terms of the squared peak field intensity and the squared beam width as functions of z

$$A_m^2(z) \equiv a_m(z) = \frac{A_{mo}^2}{f(z)} \tag{32}$$

$$w^2(z) \equiv -\frac{1}{2a_2(z)} = w_0^2 f(z) \tag{33}$$

where

$$f(z) = e^{\frac{4}{k}g(z)}$$

$$= \left[\frac{1}{R^2} - \frac{\beta_2 A_{mo}^2}{\epsilon_p w_o^2}\right] z^2 + \frac{2}{R} z + 1 \tag{34}$$

Setting $f(z) = 0$, we can determine the focal length as

$$z_f = \frac{\frac{A_{mo}}{w_o}\sqrt{\frac{\beta_2}{\epsilon_p}} - \frac{2}{R}}{2\left(\frac{\beta_2 A_{mo}^2}{\epsilon_p w_o^2} - \frac{1}{R^2}\right)} \tag{35}$$

where ϵ_p and β_2 have been defined in Eqs. (6) and (9), respectively. These results were obtained by Akhmanov et al. (1966) for studying the self-focusing effect in nonlinear optical medium. But the assumption of a global quadratic field intensity profile and the geometrical optical approximation are required in their work. From our above analysis, one can see that both of those are unrealistic and unnecessary for the near-axis solution. For example, in the ionospheric F-region, $n = 4.5 \cdot 10^{11}\text{m}^{-3}$, $T_e = T_i = 1000°\text{K}$, and the wave frequency is taken to be 400 MHz, $w_o = 100\text{m}$, then the

critical field intensity is found to be $A_m^c \simeq 395 V/m$. For a beam with $A_m = 10 A_m^c$, the focal length calculated from Eq. (34) is about 4.2 Km.

6. Summary and Discussion

In summary, our analysis has showed that a Gaussian beam no longer maintains its shape during the self-focusing process. A threshold or critical power is required for the self-focusing effect to overcome the natural diffraction. If the incident power is much greater than the critical power, the beam will focus at the beam center. The theoretically determined focal length represents the upper bound of the characteristic path length for the self-focusing process to accomplish. This is because we have not considered any energy absorption process that may impede or cause the saturation of the concerned self-focusing process. The fact that the phase and amplitude of the wave field vary drastically near the focal point as shown in Eqs. (25) and (32) also shed doubt on the validity of neglecting the higher-order terms in Eq. (12). The thermal effect, expected to contribute additively with the ponderomotive force to the self-focusing effect, should also be taken into account. More detailed analysis of this problem will be presented later.

References

Akhmanov, S.A., A.P. Sukhorukov and R. Khokholov, Self-focusing and self-trapping of intense light beams in a nonlinear medium. Sov. Phys. JETP,**23**, 1025, 1966.

Chiao, R.Y., E. Garmire, and C.H. Townes, self-trapping of optical beams. Phys. Rev. Lett., **13**, 479, 1964.

Kelley, P.L., Self-focusing of optical beams, Phys. Rev. Lett. **15**, 1005, 1965.

Lugovoi, V.N., and A.M. Prokhorov, Theory of the propagation of high-power laser radiation in a nonlinear medium, Sov. Phys. -Usp., **16**, 658, 1974.

Wagner, W.G., H.A. Haus, and J.H. Marburger, Large-scale self-trapping of optical beams in the paraxial ray approximation, Phys. Rev., **175**, 256, 1968.

APPENDIX B

SPECTRAL BROADENING OF VLF RADIO SIGNALS TRAVERSING THE IONOSPHERE

K.M. Groves
Research Laboratory of Electronics
Massachusetts Institute of Technology
Cambridge, Massachusetts 02139

Abstract

Nearly monochromatic signals at 13.6 kHz ±1 Hz injected from a ground-based VLF transmitter can experience a bandwidth expansion as high as 1% (~ 100 Hz) of the incident wave frequency as they traverse the ionosphere and reach satellite altitudes in the range of 600-3800 kilometers [*Bell et al.*,1983]. We investigate two different source mechanisms that can potentially result in the observed spectral broadening of injected monochromatic VLF waves. One is the nonlinear scattering of VLF signals by induced ionospheric density fluctuations that renders the nonlinear mode conversion of VLF waves into lower hybrid waves. These quasi-electrostatic modes result when the injected VLF waves are scattered by ionospheric density fluctuations with scale lengths less than $0.7(c/f_p)(f_e/f_o)^{1/2}$, where c, f_p, f_e, and f_o are the speed of light in vacuum, the plasma frequency, the electron cyclotron frequency, and the VLF wave frequency, respectively. A second mechanism involves the excitation of electrostatic waves (lower hybrid waves, low frequency quasi-modes) by the injected VLF waves. This process tends to produce a spectrally broadened transmitted pulse with peaks at a discrete set of frequencies on both sides of the nominal carrier frequency. Controlled study of the spectral broadening phenomenon by the combined operation of two (one HF and one VLF) heaters in the so-called ionospheric modification experiments is suggested.

Thesis Advisor: Dr. M. C. Lee

1. INTRODUCTION

In this paper we propose two mechanisms to explain the recently observed bandwidth expansion experienced by nearly monochromatic signals at 13.6 kHz ±1 Hz injected from a ground-based VLF transmitter as they traverse the ionosphere and reach satellite altitudes in the range of 600-3800 kilometers (Figure 1) [*Bell et al.*, 1983]. A schematic illustration of this puzzling phenomenon is shown in Figure 2.

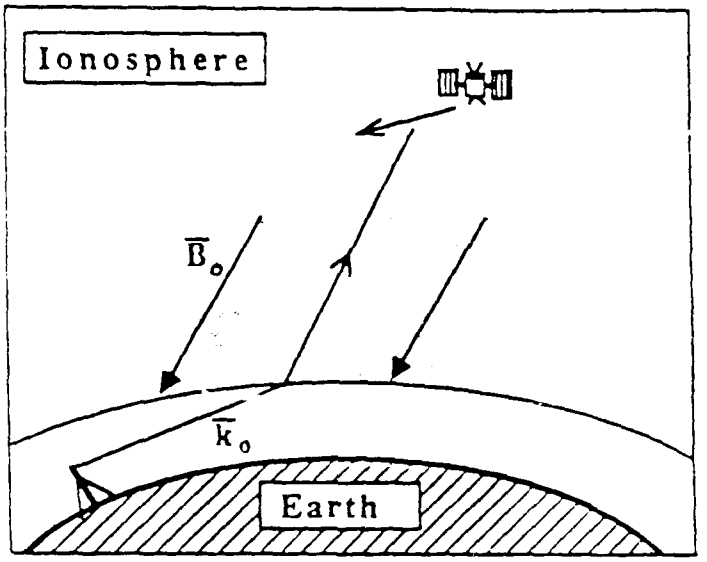

FIGURE 1. Geometry of spectral broadening observations.

FIGURE 2. Bandwidth expansion of transionospheric VLF wave

This expansion of bandwidth, which results in a proportional increase in signal-to-noise ratio, may be as large as 1% (~ 100 Hz) of the carrier frequency, and the off-carrier components are thought to be electrostatic in nature [*Inan and Bell*, 1985]. The five types of spectrally broadened transmitter signals which have been found are illustrated in Figure 3. They occur only in the presence of impulsive VLF hiss and/or a lower hybrid resonance (LHR) noise band with an irregular cutoff frequency, and only for signals whose frequencies exceed the LHR frequency at the satellite location. The observed signal at the carrier frequency is usually suppressed relative to the sidebands.

The linear scattering source mechanism was first suggested by *Bell et al.*, [1983], who hypothesized the creation of the required ionospheric density fluctuations by precipitating, low energy (< 1 kev) electrons. Such precipitation events have been accompanied by both VLF hiss and irregular LHR noise bands (McEwen and Barrington, 1967; Laaspere et al., 1971; Gurnett and Frank, 1972). Bell et al. (1983) then speculate that the broadening of the transmitted pulse spectrum results from the scattering of the initial signals from the precipitation-induced density fluctuations and the subsequent coupling into quasi-electrostatic whistler mode waves of short wavelength. The Doppler shift associated with these short wavelength modes is large enough to produce the bandwidth expansion of the signals measured on a moving satellite.

The first mechanism which we propose, presented in section 2, differs from that of Bell et al.'s in two basic aspects: 1) The density irregularities required for scattering may be induced by the injected VLF waves themselves, rather than particle precipitation [*Lee and Kuo*,1984]; 2) The proposed scattering is the nonlinear scattering of VLF signals by induced ionospheric density fluctuations that renders the nonlinear mode conversion of VLF waves into lower hybrid waves. In other words, the scattering of VLF waves by ionospheric density fluctuations causes elliptically polarized modes. The induced elliptically polarized modes may be predominantly electrostatic.

The second mechanism, outlined in section 3, produces a spectrally broadened signal

FIGURE 3. Characteristic spectra for five distinct types of broadening. After Bell et al., [1983]

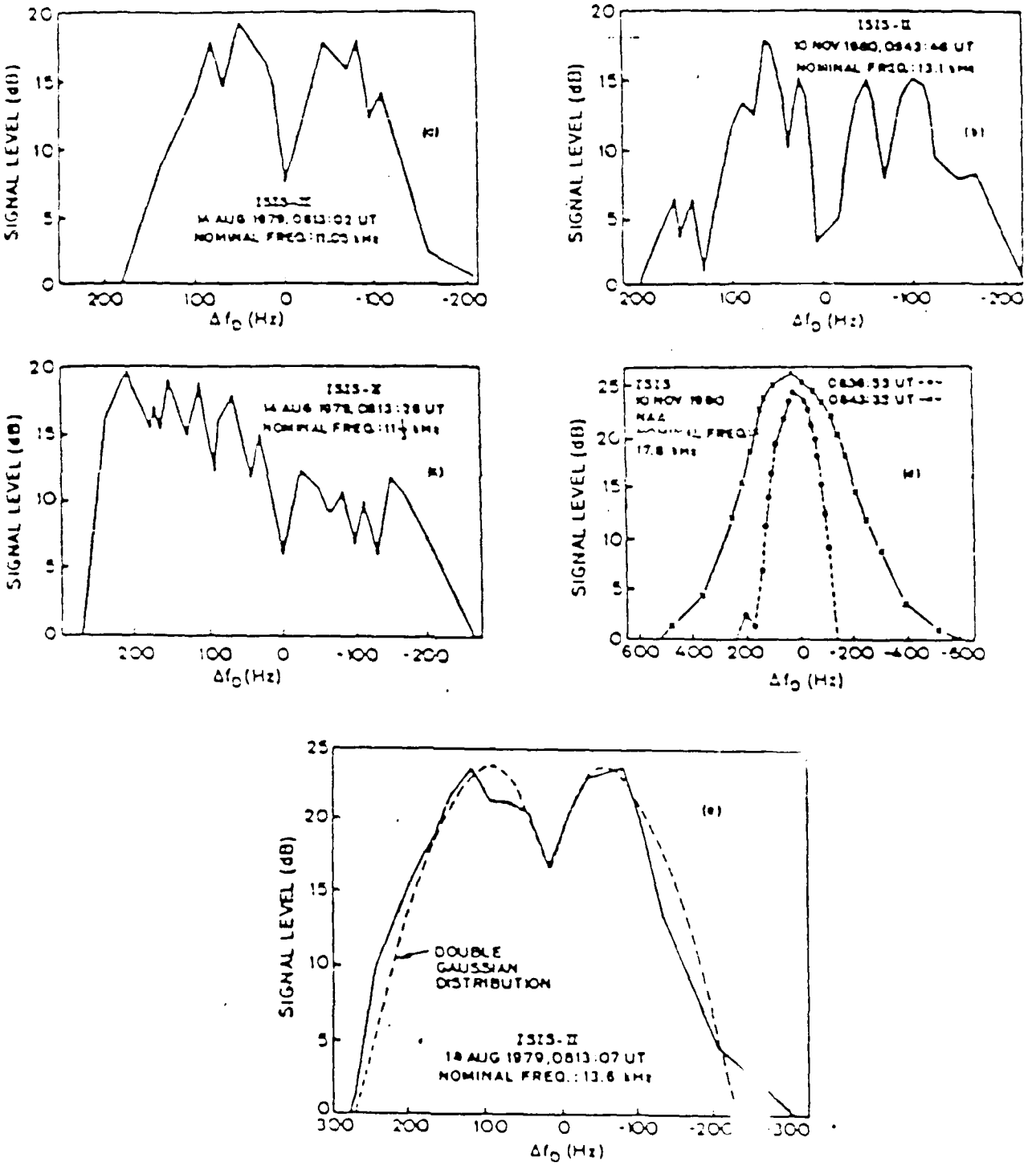

via parametric instabilities in two steps. In the first step, the injected VLF wave excites both the Stokes and anti-Stokes components of lower hybrid waves, concommitantly producing a field-aligned purely growing mode. The lower hybrid waves, acting as pump waves, can then interact with low frequency thermal-level density fluctuations, generating both backscattered and forwardscattered lower hybrid wave sidebands. The frequency shift of the sidebands relative to the lower hybrid pump wave creates a spectrally broadened signal. The processes may be summarized as follows:

$$\text{Step 1)} \quad \text{VLF} \longrightarrow LH_{1\pm} \; - \; \textit{Zero Frequency FA Mode}$$

$$\text{Step 2)} \quad \text{LH}_1 \longrightarrow LH_{2\pm} \; - \; \textit{Low Frequency FA Mode}$$

where VLF, LH, and FA stand for Very Low Frequency wave, Lower Hybrid wave, and Field Aligned, respectively. The $\pm$ - indicates that both upshifted and downshifted modes are produced. The excitation of LH waves by these processes may also result in the acceleration of both electrons and ions. A summary and conclusion follow in section 4.

2. NONLINEAR WAVE SCATTERING

Theory

A monochromatic VLF wave transmitted from a ground-based station into space has been observed to change from linear into circular polarization (i.e., whistler mode) as it travels through the neutral atmosphere into the ionosphere (Kintner et al., 1983). If a ducted whistler wave mode is considered for simplicity, the wave electric field may be represented as

$$\mathbf{E}_o = \mathrm{E}_o(\hat{\mathbf{x}} + \mathrm{i}\hat{\mathbf{y}}) \exp \mathrm{i}(\mathrm{k}_o z - \omega_o t) \qquad (1)$$

where the z axis has been taken along the geomagnetic field lines; ω_o is the transmitted wave frequency, and k_o the associated wave vector, assumed to be along the z axis for a ducted mode, as illustrated in Figure 1a. Propagating into an unperturbed ionosphere,

the whistler wave satisfies the electromagnetic wave equation

$$\nabla^2 \mathbf{E}_o - \frac{1}{c^2}\frac{\partial^2}{\partial t^2}\mathbf{E}_o = \mu_o \frac{\partial}{\partial t}\mathbf{j}_o \tag{2}$$

where $\mathbf{j}_o$ is the uniform oscillatory current driven by the incident wave field in the ionospheric plasma.

$$\mathbf{j}_o = \frac{ie^2 N_o \mathbf{E}_o}{m_e(\omega_o - \Omega_e)}$$

and e, N_o, m_e and Ω_e are the electron charge, uniform background plasma density, electron mass, and the unsigned electron cyclotron frequency, respectively.

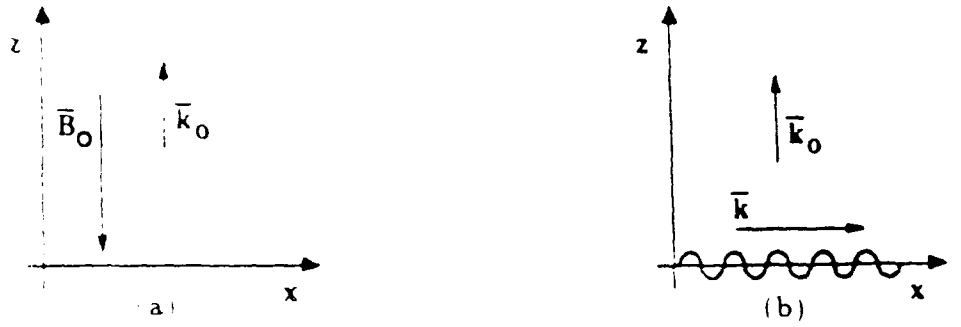

FIGURE 1 Geometry of wave propagation for a) uniform ionosphere; b) ionosphere with irregularities present

In the presence of field-aligned ionospheric density irregularities, the scattered wave, allowing for longitudinal modes, can be described by

$$\nabla(\nabla \cdot \mathbf{E}_s) - \nabla^2 \mathbf{E}_s + \frac{1}{c^2}\frac{\partial^2}{\partial t^2}\mathbf{E}_s = -\mu_o \frac{\partial}{\partial t}\delta \mathbf{j}_s \tag{3}$$

where δj_s is the [illegible] uniform current induced by the interaction of the whistler wave field with the density irregularities. We take the x axis along the direction of the density irregularities which are assumed to be of the form

$$\Delta n = \Delta \hat{n} \exp ikx \tag{4}$$

depicted graphically in Figure 4b. The nonuniform current, $\delta \mathbf{j_s}$, can then be expressed as

$$\delta \mathbf{j_s} = -e(N_o \delta \mathbf{v} - \frac{\delta n}{N_o} \mathbf{j_o}) \tag{5}$$

where δv is the induced velocity perturbation. The scattered wave field has the general form of

$$\mathbf{E_s} = (\hat{\mathbf{x}} E_x - i\hat{\mathbf{y}} E_y) \exp[i(k_o z - \omega_o t)] \tag{6}$$

Solving the wave equation together with the electron momentum equation, the scattered wave field is found to be elliptically polarized

$$\mathbf{E_s} = E_o(\delta n / N_o)\hat{\mathbf{x}} - (\hat{\mathbf{x}} - i\hat{\mathbf{y}})E_s] \exp[i(k_o z - \omega_o t)] \tag{7}$$

E_s is the amplitude of the circularly polarized component of the wave given by

$$E_s = -\frac{2\omega_{pe}^2 \omega_o}{k^2 c^2 (\omega_o - \Omega_e)} \tag{8}$$

where ω_{pe} and c are the electron plasma frequency and the speed of light in vacuum, respectively, and k is the wavenumber of the density perturbation defined by (4). Writing the scattered field in terms of the ionospheric irregularity scale length, $\lambda = 2\pi / k$. We find

$$\mathbf{E_s} = E_o \exp[ikx(\delta \tilde{n} / N_o)] \underbrace{\hat{\mathbf{x}}}_{LP} - \underbrace{(\hat{\mathbf{x}} - i\hat{\mathbf{y}})}_{CP} \frac{\lambda^2}{\lambda_c^2} \exp[i(k_o z - \omega_o t)] \tag{9}$$

where,

$$\lambda_c = \sqrt{2}\pi (c/\omega_{pe})(\Omega_e/\omega_o)^{1/2} \approx 4.4 k_o$$

The scattered field is composed of a linearly polarized (LP) part and a circularly polarized (CP) part as indicated in (9). If the ratio $(\lambda^2 / \lambda_c^2) \ll 1$ (i.e., $k \gg k_o$) the scattered wave is dominated by the linearly polarized component, which oscillates in the direction of the irregularity wavevector, $\mathbf{k}$; hence, the wave is electrostatic in nature and exhibits a broadened, enlarged wave vector spectrum relative to the incident wave. The Doppler shift frequency measured by a moving satellite will be enlarged as well.

Analysis

The condition found above for effective nonlinear scattering into quasi-electrostatic modes requires $\lambda \ll \lambda_c$. Typical plasma parameters for the upper ionosphere/lower magnetosphere region of interest are $\omega_{pe}/2\pi = 0.8$ MHz, $\Omega_e/2\pi = 0.6$ MHz. Assuming an incident frequency of $\omega_0/2\pi = 13.6$ kHz, we calculate $\lambda_c \approx 1.3$ km. The magnitude of the bandwidth expansion measured by a moving satellite due to the Doppler shift of the scattered VLF wave is

$$\Delta f = \frac{\mathbf{k_s} \cdot \mathbf{v_s}}{2\pi} \simeq \frac{v_s \cos\theta}{\lambda} \approx \frac{v_s}{\lambda} \tag{10}$$

where $\mathbf{v_s}$ is the velocity of a satellite moving across the earth's magnetic field as shown in Figure 5, and $\mathbf{k_s} = k\hat{\mathbf{x}} - k_0\hat{\mathbf{z}}$.

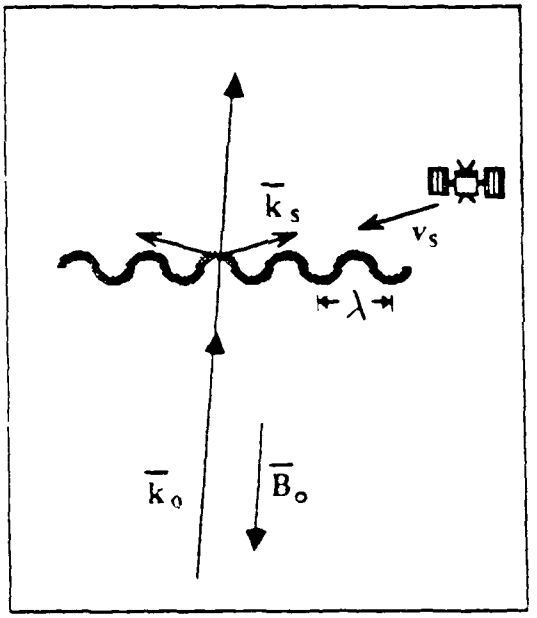

FIGURE 5. Schematic of Doppler shift phenomenon

Given $v_s \simeq 5$ km sec and $\Delta f \simeq 100$ Hz, we find $\lambda \simeq 80$m $\ll \lambda_c$, so the condition for nonlinear scattering is well satisfied. Thus we have found that ionospheric irregularities with scale lengths of several tens of meters can produce Doppler shifts of

the observed magnitude. Ionospheric irregularities can occur naturally or be created by the incident VLF waves. Particle precipitation can produce irregularities with a broad range of scale lengths in a region near the F-layer peak, about 300 km above the earth's surface. However, the reduced phase speed of the scattered quasi-electostatic wave leads to significant Landau damping of this wave mode, and the amplitude of such a wave decreases exponentially as it propagates upwards to satellite altitudes of 600–3800 km. Nevertheless, the required irregularities can be induced by intense VLF waves locally [*Lee and Kuo*, 1984]. Furthermore, these wave-induced irregularities possess a relatively narrow spectrum of scale lengths ranging from a few meters to a few tens of meters.

3. EXCITATION OF ELECTROSTATIC MODES

Parametric Excitation of Lower Hybrid Waves

In this section we discuss the proposed second mechanism responsible for the observed VLF spectral broadening that involves the parametric excitation of lower hybrid waves and ionospheric irregularities. As in the previously considered case of nonlinear scattering, the incident wave is also assumed to be a ducted whistler mode with $\mathbf{k}_o = k_o\hat{\mathbf{z}}$, propagating along the geomagnetic field lines, taken to be the z axis. Assuming the space-time dependence of the perturbations to be $\exp[i(\mathbf{k}_o \cdot \mathbf{r} - \omega t)]$, the first physical process of VLF $\rightarrow$ $LH_{1\pm}$ + Zero Frequency FA Mode can be described by the following wave frequency and wave vector matching relations:

$$\omega_{1\pm} - \omega_s = \omega_o = \omega_{1-} - \omega_s^*$$

$$\mathbf{k}_{1\pm} - \mathbf{k}_s = \hat{z}k_o = \mathbf{k}_{1-} - \mathbf{k}_s \qquad (11)$$

where the subscripts $1\pm$ and s refer to the Stokes anti-Stokes components of the high frequency lower hybrid sidebands and the field- aligned zero frequency mode, respectively. Choosing the x axis to coincide with the wave vector, $\mathbf{k}_s$, of the field-aligned modes, as shown in Figure 6a, and expressing the frequency $\omega_s = i\gamma$ ($Re\omega_s = 0$), the matching

conditions (11) may be represented by

$$\omega_{1\pm} = \omega_o \pm i\gamma$$

$$\mathbf{k}_{1\pm} = \hat{\mathbf{z}}k_o \pm \hat{\mathbf{x}}k_s \tag{12}$$

This process has been investigated in detail in *Lee and Kuo*, 1984. For the upper ionosphere in the frequency range of interest, the nonoscillatory current resulting from the beating of the density fluctuations associated with the lower hybrid waves and the electron response to the whistler pump field is found to be the dominant nonlinear effect. The scale lengths of the zero frequency modes are found to be a few tens of meters; hence, $k_s \gg k_o$.

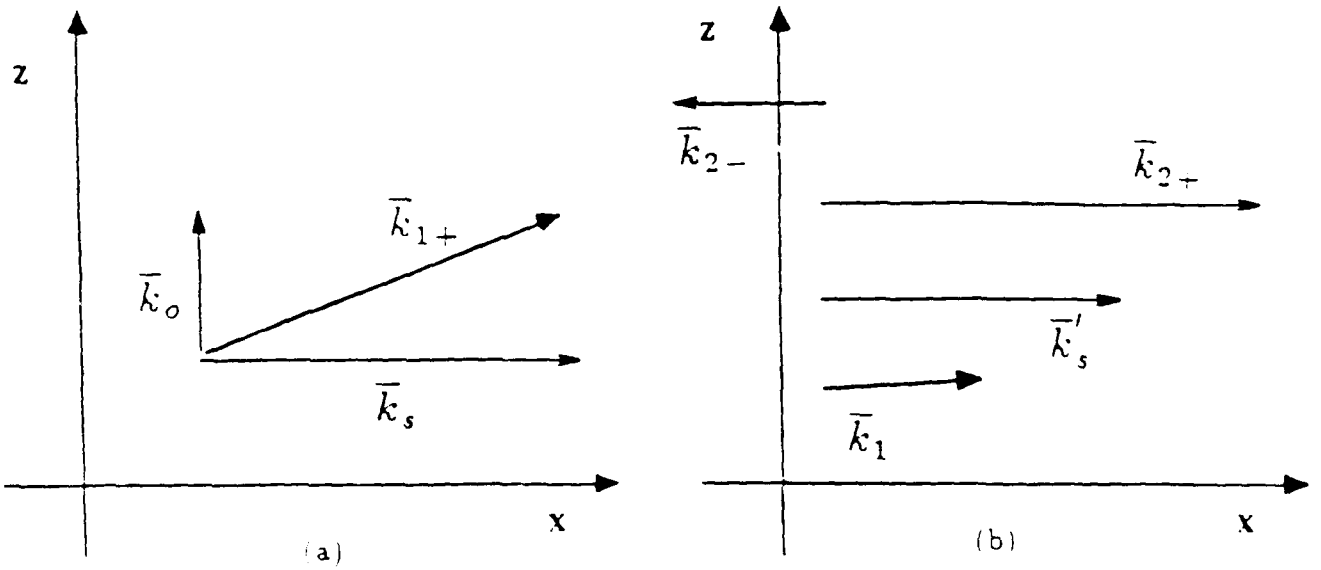

FIGURE 6. Illustration of wave vector matching relations for a) Step 1; b) Step 2

Stimulated Scattering of Lower Hybrid Waves

The lower hybrid waves generated by the first process, with wave vector and wave frequency denoted by $\mathbf{k}_1$, ω_1, respectively, can act as pump waves to produce high frequency lower hybrid sidebands ($\mathbf{k}_2, \omega_2$), and low frequency field-aligned modes ($\mathbf{k}_s, \omega_s$).

$Re\,\omega_s \ll \omega_{1i}$ via the second parametric instability described by the following matching relations,

$$\omega_{2\pm} = \omega_1 \pm \omega_s$$

$$\mathbf{k}_{2\pm} = \mathbf{k}_1 \pm \mathbf{k}_s \qquad (13)$$

where the subscripts + - refer to the anti-Stokes/Stokes components of the lower hybrid sidebands. The wave vector matching relation for this step is illustrated graphically in Figure 6b. The Stokes component of the sidebands may be chosen as an eigenmode of the plasma by setting $\mathbf{k}_s = 2\mathbf{k}_1$, which minimizes the threshold of the instability. While the backscattered sideband mode has the same scale length as the pump wave, that of the forward scattered sideband mode is one-third of the pump wavelength. The dispersion relation obeyed by the LH pump wave is given by,

$$\omega_1 = \omega_{lh}[1 - (m_i k_{1z}/m_e k_1)]^{1/2}$$

where

$$\omega_{lh} = \frac{(\omega_{pi}^2 + k_1^2 v_{ti}^2)^{1/2}}{(1 + \omega_{pe}^2/\Omega_e^2)^{1/2}}$$

is the lower hybrid resonance frequency.

The high-frequency sideband modes are driven by the beating current induced by the pump wave field on the density perturbation associated with the low-frequency mode. The nonoscillatory low-frequency mode, by contrast, is driven primarily by ion nonlinearity, including the ponderomotive force and the nonoscillatory beating current. While the ponderomotive force acts as the driving source, the nonoscillatory beating current imposes a stabilization effect on the instability.

The plasma dynamics under consideration are determined by the momentum equation,

$$m_j n_j(\partial/\partial t + \mathbf{v}_j \cdot \nabla)\mathbf{v}_j = n_j q_j(\mathbf{E} + \mathbf{v}_j \times \mathbf{B}_o) - \nabla T_j n_j \qquad (14)$$

the equation of continuity,

$$(\partial/\partial t)n_j + \nabla \cdot n_j \mathbf{v}_j = 0 \qquad (15)$$

and, in the present case of low frequency oscillations, the quasi-neutrality condition,

$$n_i = n_e \tag{16}$$

where n, q, and T represent particle density, charge, and temperature in units of energy. The subscript j refers to the particle species: i for H^- ions or e for electrons, as written explicitly in (16). Wavelike perturbations are assumed, having the form $\delta n_1, \mathbf{v}_1 \sim \exp[i(\mathbf{k}_1 \cdot \mathbf{r} - \omega_1 t)]$; $n_s, \mathbf{v}_s \sim \exp[i(\mathbf{k}_s \cdot \mathbf{r} - \omega_s t)]$; and $\delta n_\pm, \mathbf{v}_\pm \sim \exp[i(\mathbf{k}_{2\pm} \cdot \mathbf{r} - \omega_{2\pm} t)]$ where $\mathbf{k}_{2\pm}$ and $\omega_{2\pm}$ are defined by (13). Under the electrostatic approximation we may also express the electric field, $\mathbf{E}$, as the gradient of a potential function, φ. The interaction of the high frequency LH pump wave with the high frequency LH sidebands drives the low frequency field-aligned modes; the corresponding momentum equation is,

$$\omega_s m_j \mathbf{v}_{sj} = i q_j / n_o (\mathbf{v}_{sj} \times \mathbf{B}_o) - \mathbf{k}_s T_j (n_s / n_o) - i\mathbf{F}_j \tag{17}$$

where $\mathbf{F}_j$, the nonlinear ponderomotive force arising from the convective, has the form

$$\mathbf{F}_j = -i m_j [\mathbf{k}_o \cdot (\mathbf{v}^*_{-j} \mathbf{v}_{oj} - \mathbf{v}_{-j} \mathbf{v}^*_{oj}) - \mathbf{k}_+ \cdot \mathbf{v}^*_{oj} \mathbf{v}_{-j} - \mathbf{k}_- \cdot \mathbf{v}_{oj} \mathbf{v}^*_{-j}]$$

Applying (16) to the equation of continuity, we obtain

$$\omega_s (n_s / n_o) = \mathbf{k}_s \cdot (\mathbf{v}_{se} - \mathbf{v}^{nl}_e) = \mathbf{k}_s \cdot (\mathbf{v}_{si} + \mathbf{v}^{nl}_i) \tag{18}$$

where the induced electron and ion nonoscillatory beating currents are defined by

$$n_o \mathbf{v}^{nl}_j = \delta n^*_{oj} \mathbf{v}_{+j} + \delta n_{oj} \mathbf{v}^*_{-j} + \delta n_{-j} \mathbf{v}^*_{oj} + \delta n^*_{-j} \mathbf{v}_{oj} \tag{19}$$

The velocity responses of the electrons and ions to the lower hybrid wave fields in (19) may be found by solving the linearized momentum equations for both species; the result is

$$\mathbf{v}_{eo,\pm} = -i\mathbf{k}_{o,\pm} \times [\hat{\mathbf{x}} + i\hat{\mathbf{y}}(\omega_{o,\pm}/\Omega_e) - i\hat{\mathbf{z}}(k_{oz}\Omega_e / k_{o\perp}\omega_{o,\pm})] \times [(e\Phi_{o,\pm}/m_e\Omega_e) - (v^2_{te}\delta n_{eo,\pm}/n_o\Omega_e)] \tag{20}$$

$$\mathbf{v}_{io,\pm} = i\mathbf{k}_{o,\pm} \times [\hat{\mathbf{x}}(\Omega_i/\omega_{o,\pm} - i\hat{\mathbf{y}} - i\hat{\mathbf{z}}(k_{oz}/k_{o\perp})] \times [(e\Phi_{o,\pm}/m_i\omega_{o,\pm}) - (v^2_{ti}\delta n_{io,\pm}/n_o\omega_{o,\pm})] \tag{21}$$

The equation of continuity can then be linearized and solved for the corresponding density perturbations,

$$\delta n_{eo,\pm} = (n_o e/m_e\Omega_e^2)k_{o,\pm\perp}^2\{(1 - k_{oz}^2\Omega_e^2/k_{o,\pm}^2\omega_{o,\pm}^2)\phi_{o,\pm}$$
$$- \delta_{o,\pm}(k_{o,\pm}/k_{\pm\perp})(\omega_o/\omega_\pm)(1 - k_{oz}^2\Omega_e^2/k_{o,\pm}^2\omega_o^2)$$
$$\times (1 - k_o\omega_{s\pm}/k_s\omega_o)[1 + (k_{o,\pm}^2 v_{te}^2/\Omega_e^2)(1 - k_{oz}^2\Omega_e^2/k_{o,\pm}^2\omega_o^2)]$$
$$\times \phi_o(n_{s\pm}/n_o)\}[1 + (k_{o,\pm\perp}^2 v_{te}^2/\Omega_e^2)(1 - k_{oz}^2\Omega_e^2/k_{o,\pm}^2\omega_{o,\pm})]^{-1} \quad (22)$$

$$\delta n_{io,\pm} = (n_o e/m_i\omega_{o,\pm}^2)k_{o,\pm\perp}^2[\phi_{o,\pm} - \delta_{o,\pm}(k_o/k_\pm)(\omega_\pm/\omega_o)$$
$$\times (1 - k_o\omega_{s\pm}/k_s\omega_o)(1 - k_o^2 v_{ti}^2/\omega_o^2)\phi_o(n_{s\pm}/n_o)]$$
$$\times (1 - k_{o,\pm\perp}^2 v_{ti}^2/\omega_{o,\pm}^2)^{-1} \quad (23)$$

where $\delta_o = 0$ and $\delta_\pm = 1$. Substituting these first-order results and solving (17)-(19) together with a similar set of equations governing the interaction of the LH pump wave and the low frequency field-aligned mode, and assuming $\omega_s \ll \omega_o$, the following dispersion relation is obtained

$$a\omega_s^3 + b\omega_s^2 - c\omega_s + d = 0 \quad (24)$$

where

$$a = 2\Lambda(k_o k_s v_{ti}^2/k_{sz}^2 C_s^2)[(1 + k_s^2 C_s^2/\Omega_i^2)/\omega_1(1 - \omega_{pe}^2/\Omega_e^2)]$$
$$b = 1 - \Lambda^2(1 + k_s^2 C_s^2/\Omega_i^2)k_1^2(k_s^2 - 4k_1^2)v_{ti}^4/k_{1z}^2 C_s^2\omega_1^2(1 - \omega_{pe}^2/\Omega_e^2)^2$$
$$c = [k_{sz}^2 C_s^2/(1 + k_s^2 C_s^2/\Omega_i^2)]a$$
$$d = \tfrac{1}{2}\Lambda[(v_{ti}^2/C_s^2)/\omega_1^2(1 + \omega_{pe}^2/\Omega_e^2)^2](k_s^2 v_{\phi i}^2\omega_1^2\{[\eta/\alpha(1 - k_1^2 v_{ti}^2/\omega_1^2)$$
$$- \alpha(\omega_1^2 - k_1^2 v_{ti}^2)/\Omega_e\Omega_i] - 4\eta(k_1^2 v_{te}^2/\Omega_e^2)(k_s - 2k_1)/k_s(1 - k_1^2 v_{ti}^2/\omega_1^2)\}$$
$$- \tfrac{1}{2}\Lambda k_s^2(k_s^2 - 4k_1^2)C_s^2 v_{ti}^2)$$
$$\Lambda = 1 - \omega_{pe}^2/\Omega_e^2 - \eta(\omega_{pe}^2 - 10k_1^2 v_{te}^2)/\Omega_e^2 \quad (25)$$
$$\eta = 1 - k_{1z}^2\Omega_e^2/k_1^2\omega_1^2$$

$$\alpha = \eta_i(1 - k_{1z}^2 v_{te}^2/\omega_1^2 - k_1^2 v_{te}^2/\Omega_e^2)$$

$$v_{te}^2 = 3T_e/m_e$$

$$v_{ti}^2 = 3T_i/m_i$$

Substituting $\omega_s = \omega_r - i\gamma$ into (24), two equations for the growth rate, γ, and the real frequency, ω_r, are obtained.

$$\gamma^2 = \{d/(b - 2a\omega_r)\} - \omega_r^2 \tag{26}$$

$$(b - 2a\omega_r)^3 - b(b - 2a\omega_r)^2 - ac(b - 2a\omega_r) - a^2 d = 0 \tag{27}$$

Setting $\gamma = 0$ to determine the threshold of the instability, (26) and (27) may be solved for the coefficient, d, giving

$$d = 2a\{(b/3a)^2 - c/3a\}\{(b/3a)^2 - c/3a\}^{1/2} - \{(b/3a)^3 - bc/6a^2\} \tag{28}$$

Equating this result with the expression in (25), we find the threshold condition of the instability requires

$$v_{oi}^2 \geq v_{thi}^2 \simeq \{\tfrac{4}{3}(k_{sz}C_s/\omega_1)(2k_1/k_s)(1 - \omega_{pe}^2/\Omega_e^2)$$

$$\times (1 - h)^{3/2} - \tfrac{3}{2}h^{1/2}(1 - 2h/3)\}/\{3(1 + k_s^2 C_s^2/\Omega_i^2)\}^{\frac{1}{2}}\}C_s^2 \times \{\eta/\alpha - \alpha\omega_1^2/\Omega_e\Omega_i\}^{-1} \tag{29}$$

where $v_{oi} = eE_1/m_i\omega_1$ is the ion quiver velocity, $h = b^2/3ac$, and $C_s = (T_e + T_i)/m_i)^{1/2}$ is the acoustic speed in the ionospheric plasma. When the lower hybrid pump field strength is sufficient to produce quiver velocities in excess of that required by (29), positive growth rates for the instability occur.

Characteristics of the Instability

This mechanism has been analyzed for typical plasma parameters in the upper ionosphere lower magnetosphere, namely for: $\omega_{pe}/2\pi = 0.65MHz$; $\Omega_e/2\pi = 0.55MHz$; $\omega_{pi}/2\pi = 15KHz$; $\Omega_i/2\pi = 330Hz$; $m/M_i(H^+) = 5.45 \times 10^{-4}$; $T_e = T_i = 1000°K$. The analysis was carried out in the spectral range about $k_s \simeq 2k_0$, consistent with previous

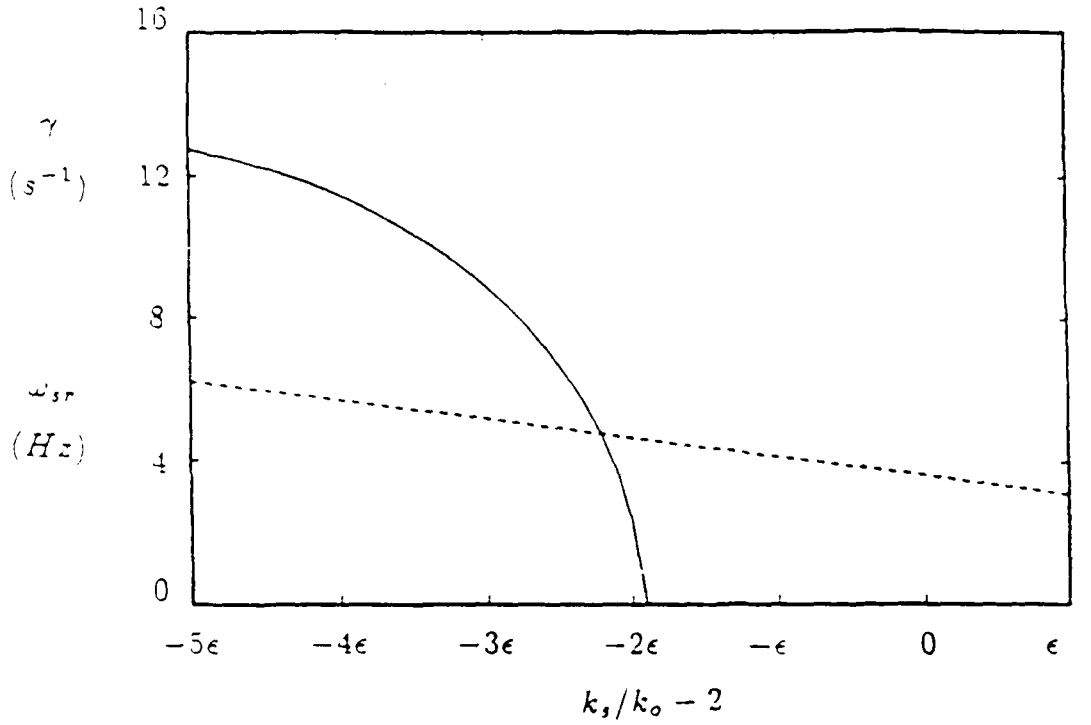

FIG. 7. Spectral dependence of the instability growth rate (solid line) and the real frequency of the low-frequency quasi-mode (dotted line) when $v_{oe} = C_s$: where $\epsilon = 10^{-2}$.

assumptions. Illustrated in Figure 7 is the spectral dependence of both the growth rate of the instability and real frequency of the low frequency, field-aligned mode. The real frequency of this low frequency mode corresponds to the detected broadening of the VLF wave frequency by the orbiting satellite as shown by the frequency matching condition, (13). The plots in Figure 7 were calculated by solving the complete dispersion relation, (22) and (23), for the instability assuming an electron quiver velocity, $v_{oe} \simeq v_{oi}(\omega_o/\Omega_i) = C_s$. The growth rate, γ, goes to zero near $k_s = 2k_o(1 - \epsilon)$, because the threshold electron quiver velocity exceeds C_s at this point. As can be seen in Figure 6, the growth time of the instability is about 100 *ms*; for pulse lengths of the order of one second, significant growth can occur. The growth rate and spectral range of the instability increase linearly with the pump power

as $v_{oe} \geq C_s \sqrt{2}$. Although the calculated magnitude of the broadening is less than the observed values of 100 Hz, it increases by a factor of two for an order of magnitude increase in the electric field strength of the lower hybrid pump wave.

4. SUMMARY AND CONCLUSION

In summary, we have investigated two possible source mechanisms that can be responsible for the observed spectral broadening of injected VLF waves. In the presence of ionospheric irregularities with scale lengths of several tens of meters, the nonlinear scattering of the VLF waves off these density irregularities can produce quasi-electrostatic modes with larger wave vectors which give rise to the apparent spectral broadening through the Doppler shift observed by the moving satellite; the broadening produced through this mechanism is of the same magnitude as the observed values. The amplitude of the quasi-electrostatic modes depends linearly on the amplitude of the ionospheric irregularities. One possible source of the field-aligned ionospheric irregularities is particle precipitation *Bell. et al.*, 1983). However, irregularities with the required scale lengths can also be induced

locally by the VLF waves themselves via the parametric instability described by *Lee and Kuo*, 1984.

Spectral broadening of the incident wave packet may also stem from the second mechanism, which involves the parametric excitation of lower hybrid waves and low frequency quasi-modes. The frequency shift resulting from this process is generally less than the observations. However, it is significant and it increases with the field intensity of the lower hybrid pump wave. These two suggested mechanisms can contribute additively to the observed spectral broadening of injected VLF waves reported by *Bell, et al.*, [1983] and others. The broadening introduced by this mechanism is significant in that it produces a wave frequency spectrum which exhibits suppressed field intensity at the carrier frequency and enhanced intensity at a discrete set of frequencies on either side of the carrier frequency; such spectra are frequently observed. Furthermore, the lower hybrid waves excited by this mechanism have enlarged wave vectors, so apparent broadening due to the Doppler effect comparable to that calculated in the first mechanism is expected.

Another interesting phenomenon associated with the excited LH waves is the acceleration of both ions and electrons in the ionosphere. The LH pump wave generated in the first step of the mechanism has a relatively large phase velocity and can interact effectively only with electrons in the tail of the velocity distribution function. By contrast, the phase velocity of the forwardscattered LH sideband wave generated in the second step of the mechanism is one-third of the pump wave phase velocity, and the parallel (perpendicular) component is within an order of magnitude of the electron (ion) thermal velocity. Thus, the upshifted LH wave may accelerate bulk electrons and ions along and across the geomagnetic field lines, respectively.

The proposed mechanisms can be tested in the so-called ionospheric modification experiments with the combined operation of two heaters in the following scenario, depicted in Figure 5. Initially, a high frequency (HF) heater wave is transmitted from the ground to illuminate the ionosphere, producing short (meter)-scale field-aligned ionospheric

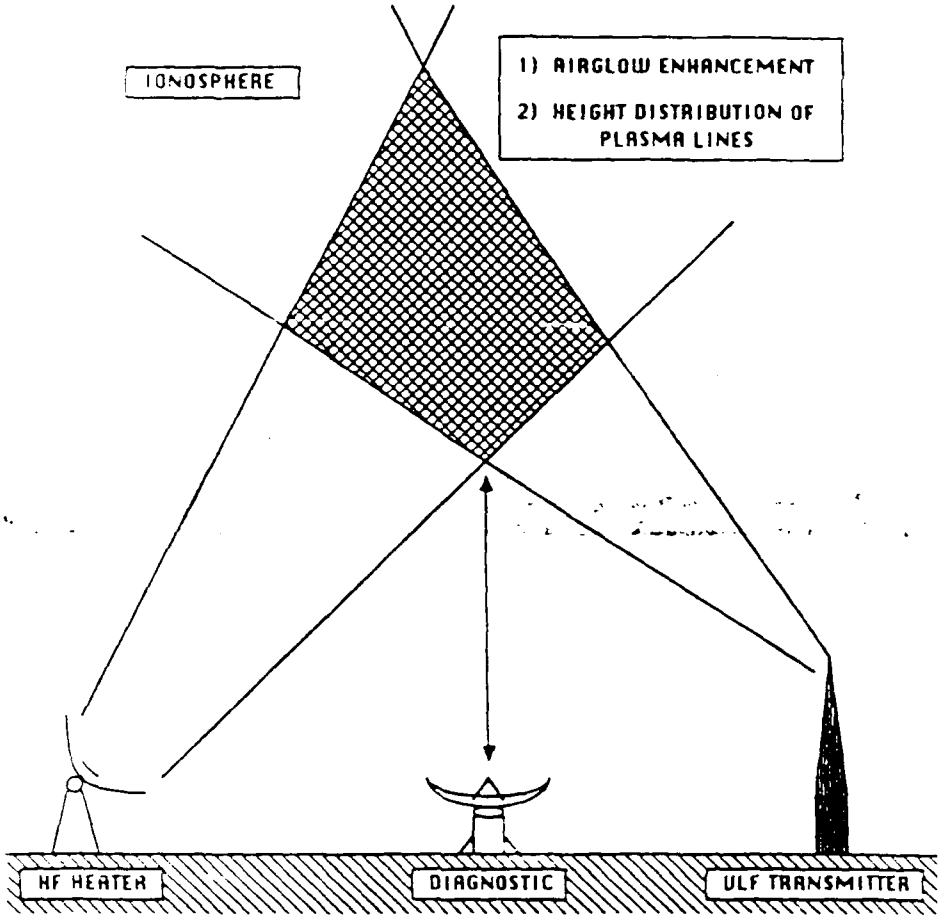

FIGURE 8. Ionospheric Modification Experiment

irregularities. The subsequent injection of a VLF wave through the HF wave-modified ionospheric region will induce lower hybrid wave modes via either nonlinear scattering off ionospheric irregularities or parametric instabilities, as elucidated in the previous sections. The induced lower hybrid waves can effectively accelerate electrons and thereby heat the ionospheric plasma. Physical observables associated with this heating include airglow enhancement (e.g., 6300 Å, 5577 Å, and shorter wavelengths) and a broad height distribution of enhanced plasma lines. In addition, backscatter radar measurements can be used to monitor the expected intensification of the field-aligned ionospheric density irregularities by the VLF waves.

References

Bell, T. F., H. G. James, U. S. Inan, and J. P. Katsufrakis, The Apparent Spectral Broadening of VLF Transmitter Signals During Transionospheric Propagation, *J. Geophys Res.*, 88, 4813-4840, 1983.

Carlson, H. C., V. B. Wickwar, and G. P. Mantas, Observations of Fluxes of Suprathermal Electrons Accelerated by HF Excited Instabilities, *J. Atmos. Terr. Phys.*, 44, 1089, 1982.

Gurnett, D. A., and L. A. Frank, VLF Hiss and Related Plasma Observations in the Polar Magnetosphere, *J. Geophys. Res.*, 77, 172, 1972.

Inan, U. S., and T. F. Bell, Spectral Broadening Of VLF Transmitter Signals Observed on DE 1: A Quasi-Electrostatic Phenomenon?, *J. Geophys. Res.*, 90, 1771-1775, 1985.

Kintner, P. M., R. Brittain, M. C. Kelley, D. L. Carpenter, and M. J. Rycroft, In Situ Measurements of Transionospheric VLF Waves, *J. Geophys. Res.*, 88, 7065, 1983.

Laaspere, T., W. C. Johnson, and L. C. Semprebon, Observations of Auroral Hiss, LHR Noise and Other Phenomena in the Frequency Range 20 Hz-540 KHz on OGO 6, *J. Geophys. Res.*, 76, 4477, 1971.

Lee, M. C., and S. P. Kuo, Production of Lower Hybrid Waves and Field-Aligned Density Striations by Whistlers, *J. Geophys. Res.*, 89, 10873-10880, 1984.

McEwen, D. J., and R. E. Barrington, Some Characteristics of the Lower Hybrid Resonance Noise Bands Observed by the Alouette I Satellite, *Can. J. Phys.*, 45, 13, 1967.

Acknowledgements. This work was supported by NASA contract NAG5-889, Lincoln Lab contract, and RADC contract through University of Dayton.

APPENDIX C

IONOSPHERIC MODIFICATIONS BY TWO HEATER WAVES

Abstract

The ionospheric modification caused by an HF or MF heater wave can be enhanced with the subsequent illumination of the ionosphere by a powerful VLF wave. The proposed scenario of ionospheric modifications by the two heater waves is based upon the following physical processes. Let the HF or MF heater be operated in a pulse-wave mode to assure the excitation of short- rather than large-scale ionospheric density irregularities. These excited ionospheric density striations can effectively scatter the VLF wave into a lower hybrid wave via the nonlinear mode conversion provided that the scale lengths of ionospheric irregularities are much less than the wavelength of the VLF wave. For example, the wavelength of a VLF wave at the frequency of 10 kHz is of the order of 500 meters in the ionospheric F region. The preferential excitation of meter-scale ionospheric irregularities by the HF or MF heater wave can provide the subsequently injected VLF wave with a favorable condition for the nonlinear mode conversion. These density striations, in fact, can also be intensified by the powerful VLF wave via a plasma instability that can concomitantly generate lower hybrid waves. The ionosphere modified by the two heater waves is expected to have intense lower hybrid waves and short-scale ionospheric density striations. These VLF wave-produced electrostatic waves can effectively heat the ionospheric plasma. Enhanced modification effects in, for instance, airglow and height distribution of plasma lines are expected. The proposed experiment can provide the controlled study of the spectral broadening effect of propagating VLF waves.

1. Introduction

As discussed in Groves et al. 1987 at the 1987 Ionospheric Effects Symposium, VLF waves can be nonlinearly scattered into lower hybrid waves by short-scale ionospheric density irregularities. VLF waves, if intense enough, can also excite lower hybrid waves and ionospheric irregularities via parametric instabilities (Lee and Kuo, 1984). Based upon these theoretical works, we propose an experimental scheme for ionospheric heating by two heater waves. One is an HF or MF heater wave and the other one is a VLF heater wave.

The proposed scheme is as follows: illumination of the ionosphere by an HF or MF wave first and, then, a VLF wave subsequently (see Figure 1). It has been known both theoretically and experimentally that short-scale (i.e., less than a few meters) ionospheric irregularities can be excited within a second by HF heater waves, while it takes tens of seconds or longer for large-scale (say, hundreds of meters and longer) ionospheric irregularities to be generated (see, e.g., Fejer, 1979 and Gurevich, 1978 for a review). As shown in Groves et al. 1987 and elaborated in Section 2 of this paper, short-scale ionospheric density striations can effectively cause the nonlinear scattering of VLF waves into lower hybrid waves. Hence, we only need to operate the HF or MF heater in pulsed mode to assure the excitation of meter-scale ionospheric irregularities. During the vertical ionospheric heating, the HF heater wave frequencies should be less than the FOF2 for overdense heating of the ionospheric F region. When an MF heater is used, the wave frequency is required to match the local electron gyrofrequency in the ionosphere to produce short-scale ionospheric irregularities via electron cyclotron heating (Lee et al., 1986).

The proposed experiment has dual purposes: (1) enhanced ionospheric modifications by the combined operation of two heater waves, and (2) controlled study of the spectral broadening of VLF waves. The suggested diagnoses for the expected ionospheric effects shall be discussed in Section 3. In principal, the two mechanisms elucidated in Groves et al. 1987 can be experimentally distinguished.

2. Heater Waves-Induced Ionospheric Effects

Various plasma instabilities can be excited by HF heater waves during overdense ionospheric heating. In less than a second, short-scale ionospheric density striations can be generated concomitantly with Langmuir waves, upper hybrid waves etc. It requires tens of seconds for the generation of large-scale ionospheric irregularities by self-focusing instability or thermal filamentation instability. Large-scale irregularities can give rise to phase and amplitude scintillation of beacon satellite signals. These wave interference patterns may not be associated with significant attenuation of the radio signals. By contrast, the short-scale irregularities are able to cause anomalous absorption of the radio signals via nonlinear scattering that converts electromagnetic wave energy into electrostatic wave energy (eventually, plasma kinetic energy) in the ionosphere.

Basically, short-scale ionospheric irregularities induced by an HF or MF heater wave can scatter the circularly polarized VLF wave into an elliptically polarized wave. A linearly polarized component of the scattered wave is introduced by the field-aligned ionospheric irregularities. In other words, the scattered whistler (VLF) wave field is composed of two parts:

$$\vec{E}_s = \exp i(k_0 z - \omega_0 t)(\hat{i}z + i\gamma E_{cp} - \gamma E_{lp}) \qquad (1)$$

where E_{cp} and E_{lp} represent the wave field intensities of the circularly polarized component and the linearly polarized component, respectively. For simplicity, a ducted whistler wave propagating along the z direction has been assumed. E_{cp} and E_{lp} are found to be related by

$$E_{lp} = 2i\frac{\lambda}{\lambda_0}E_{cp} \qquad (2)$$

where λ and λ_0 are the wavelength of ionospheric irregularities and the wavelength of the whistler wave respectively. If a VLF wave at the frequency of 10 kHz is injected, and the ionospheric conditions are assumed to be f_c electron cyclotron frequency = 1.3 MHz and f_p electron plasma frequency = 5 MHz, the whistler wavelength in the ionosphere is found to be about 500 meters. According to Equation (2), E_{lp} dominates over E_{cp} provided that $\lambda \gg \lambda_0$. Hence, meter-scale irregularities produced by HF or MF heater wave can effectively render the nonlinear mode conversion of a VLF (whistler) wave into a lower hybrid wave. The parallel and perpendicular wave vectors of the lower hybrid wave are identical to the wave vector of the ducted whistler wave and that of the field aligned ionospheric irregularities, respectively.

While the nonlinear scattering process occurs at any field intensity of the incident VLF wave, parametric instabilities can be triggered by intense enough VLF waves as suggested in Lee and Kuo 1984 and Groves et al. 1987. Short-scale ionospheric irregularities associated with zero-frequency modes can be excited via parametric decay of lower hybrid waves by the VLF waves. The excited lower hybrid waves grow and may excite a second parametric instability that generates daughter lower hybrid waves and low-frequency

ionospheric irregularities of the order of a few herts. Therefore, the HF or MF heater wave-induced short-scale ionospheric irregularities can be further strengthened by the VLF heater waves. It should be mentioned that zero-frequency modes behave as a standing wave pattern, whereas low-frequency field-aligned modes can propagate across the earth's magnetic field.

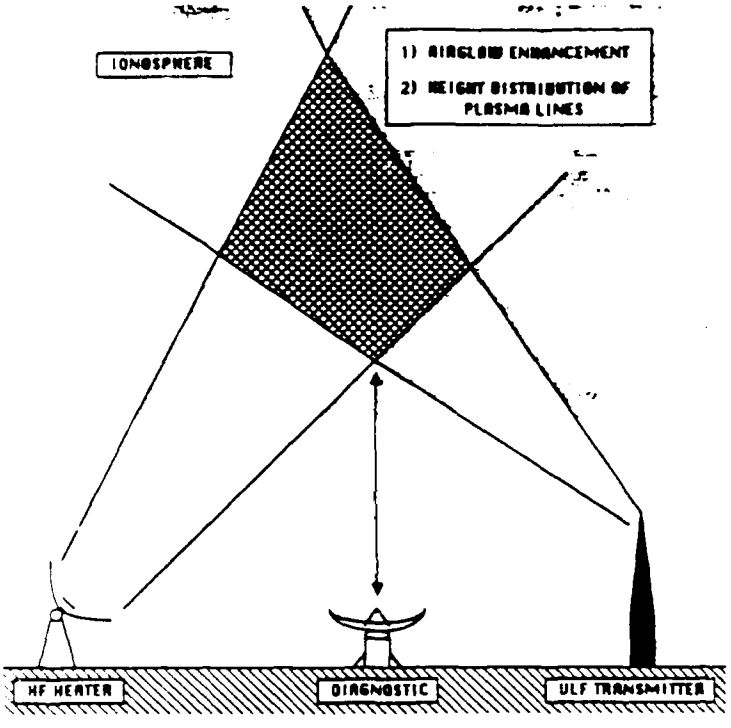

Figure 1. The proposed experiment: illumination of the ionosphere by an HF or MF wave first and, then, a VLF wave subsequently

3. Diagnosis of Expected Ionospheric Effects

It is generally believed that spread F echos in ionograms and scintillation phenomena are caused by large-scale (say, hundreds of meters) ionospheric irregularities. The generation of large-scale ionospheric density irregularities, therefore, can be sensed by ionosondes and scintillation measurements of radio stars or beacon satellite signals. By contrast, the presence of field-aligned short-scale (a few meters and less) irregularities can be detected by backscatter radars.

Backscatter radar measurements can also be made for detecting the excited lower hybrid waves when the radar's beam angle is 90° with respect to the earth's magnetic field. The recorded incoherent backscatter radar spectrum should look like a double-humped ion spectrum peaking at the lower hybrid wave frequency. Since lower hybrid waves can accelerate electrons effectively along the geomagnetic field, airglow enhancement due to the impact excitation of neutrals by energetic electrons can be expected. Measurements of airglow at 6300 Å (red), 5577 Å (green), and even shorter wavelengths may possibly be observed. In addition, the technique described in Carlson et al. 1982] for finding the height distribution of enhanced plasma lines is capable of distinguishing further the electron acceleration by Langmuir waves and lower hybrid waves that are produced, respectively, by HF and VLF heater waves.

4. Comments on the Proposed Experiments

There are several ionospheric heating facilities operated at the frequencies of a few MHz in the HF or MF band in the U.S.A., Europe, and the U.S.S.R. VLF transmitters have been used at different locations for the study of wave-particle interactions in the magnetosphere. However, it may not be possible to use the existing HF (or MF) and VLF transmitters for the proposed experiments. Since VLF waves in a narrow frequency band can be generated by lightning storms, the experiments can be carried out with available ionospheric heating facilities during lightning storms. It is not necessary to have lightning storms occurring nearby. If lightning occurs at the conjugate location in the opposite hemisphere, the lightning-induced VLF waves can propagate in ducted whistler wave modes and bounce back and forth for several cycles before they die out.

For the controlled study of the spectral broadening of VLF waves, the experiments require an air-borne VLF wave detector carried by a moving satellite or a rocket, flying through the ionosphere that has been modified by an HF or MF heater and a VLF heater. The predicted spectral broadening effect will be most prominent if the aircraft moves across the geomagnetic field perpendicularly.

References

Carlson, H.C., V.B. Wickwar, and G.P. Mantas, Observation of fluxes of suprathermal electron accelerated by HF excited instabilities, *J. Atmos. Terr. Phys.*, **44**, 1089, 1982.

Fejer, J.A., Ionospheric modification and parametric instabilities, *Rev. Geophys. Space Phys.*, **17**, 135, 1979.

Groves, K.M., M.C. Lee, and S.P. Kuo, Mechanisms leading to the spectral broadening of transmitted VLF signals, *Proceedings of Ionospheric Effects Symposium*, Springfield, Virginia, May 5-7, 1987.

Gurevich, A.V., Nonlinear phenomena in the ionosphere, Physics and Chemistry in Space 10, Springer-Verlag, 1978.

Lee, M.C. and S.P. Kuo, Production of lower hybrid waves and field-aligned density striations by whistlers, *J. Geophys. Res.*, **89**, 10873, 1984.

Lee, M.C., J.A. Kong, and S.P. Kuo, On the resonant ionospheric heating at the electron gyrofrequency, *Proceedings of the International Symposium on Modification of the Ionosphere by Powerful Radio Waves*, Suzdal, Moscow, U.S.S.R., September 9-12, 1986.

MISSION
of
Rome Air Development Center

RADC plans and executes research, development, test and selected acquisition programs in support of Command, Control, Communications and Intelligence (C^3I) activities. Technical and engineering support within areas of competence is provided to ESD Program Offices (POs) and other ESD elements to perform effective acquisition of C^3I systems. The areas of technical competence include communications, command and control, battle management information processing, surveillance sensors, intelligence data collection and handling, solid state sciences, electromagnetics, and propagation, and electronic reliability/maintainability and compatibility.

END

DATE

FILMED

1-90

DTIC